Journal of Power Sources 196 (2011) 10280–10288

Contents lists available at ScienceDirect

Journal of Power Sources

journal homepage: www.elsevier.com/locate/jpowsour

Microfibrillated cellulose as reinforcement for Li-ion battery polymer electrolytes with excellent mechanical stability

A. Chiappone[a,*], Jijeesh R. Nair[a], C. Gerbaldi[b,**], L. Jabbour[c], R. Bongiovanni[a], E. Zeno[d], D. Beneventi[c], N. Penazzi[a]

[a] Department of Materials Science and Chemical Engineering, Politecnico di Torino, C.so Duca degli Abruzzi 24, 10129 Turin, Italy
[b] Center for Space Human Robotics @Polito, Italian Institute of Technology, Corso Trento 21, 10129 Turin, Italy
[c] UMR 5518 CNRS-Grenoble-INP, Domaine Universitaire, 461 rue de la Papeterie, BP 65, 38402 St. Martin d'Hères, France
[d] Centre Technique du Papier (CTP), Domaine Universitaire, B.P. 251, 38044 Grenoble Cedex 9, France

ARTICLE INFO

Article history:
Received 22 March 2011
Received in revised form 13 June 2011
Accepted 5 July 2011
Available online 12 July 2011

Keywords:
Composite polymer electrolyte
Methacrylate
Photo polymerisation
Cellulose
Lithium battery
Mechanical property

ABSTRACT

Methacrylic-based thermo-set gel-polymer electrolyte membranes obtained by a very easy, fast and reliable free radical photo-polymerisation process and reinforced with microfibrillated cellulose particles are here presented. The morphology of the composite electrolytes is investigated by scanning electron microscopy and their thermal behaviour (characteristic temperatures, degradation temperature) are investigated by thermo-gravimetric analysis and differential scanning calorimetry. The composite membranes prepared exhibit excellent mechanical properties, with a Young's modulus as high as about 80 MPa at ambient temperature. High ionic conductivity (approaching 10^{-3} S cm^{-1} at 25 °C) and good overall electrochemical performances are maintained, enlightening that such specific approach would make these hybrid organic, cellulose-based composite polymer electrolyte systems a strong contender in the field of thin and flexible lithium based power sources.

1. Introduction

Nowadays, research efforts are focused on the development of polymer systems showing high ionic conductivity at ambient and/or sub ambient temperatures, good mechanical properties and stable performances since they find practical applications as electrolytes in high energy density, thin and lightweight secondary Li-ion batteries [1–3]. Particularly with the recent advances in the technology of emerging high-end portable applications, like bendable electronic devices [4,5], there is a huge demand for flexible and extra-thin batteries to power them. Such batteries are also being extensively considered to fit the hollow spaces of future electric vehicles [6–8] and aerospace systems [9]. In this respect, the need of a low cost, green, safe and up-scalable production process becomes fundamental for the sustainable mass production of the next generation energy storage systems.

The potential of nano- and micro-composites in various sectors of research and application is promising and is attracting increasing investments [10]. Native cellulose and chitin fibres are made up of smaller and mechanically stronger long thin filaments, called microfibrils, consisting of alternating crystalline and non-crystalline domains. When using cellulose, this material is usually called microfibrillated cellulose. Microfibrillated cellulose (MFC) particles are easily available and biodegradable; they show stiffness, impressive mechanical properties and reinforcing capability, low weight and their preparation process is easy, low cost and does not involve chemical reactions [11,12]. For all these reasons, nano-scale cellulose fibre materials have the potential to significantly reinforce polymers at low filler loadings and serve as promising candidates for bio-composite production [13–15].

A broad range of applications of cellulose fibres exists, even if a high number of unknowns remain to date. Cellulose nano-whiskers have been deeply studied and their addition to polymer matrices gave excellent results in terms of mechanical properties [16], but the process of extracting single crystal whiskers from plants is time consuming and very costly, despite the abundance and low price of the raw materials. Instead, microfibrillated cellulose nanoparticles, first studied by Herrick et al. [17] and Tubark et al. [18] in the early 1980s, are obtained through a homogenization of the paper pulp at high shear: an easy process that does not involve chemical reactions. The cellulose particles obtained have a diameter ranging between 10 and 100 nm, length in the microscale and

* Corresponding author. Tel.: +39 011 090 4656; fax: +39 011 090 4699.
** Corresponding author. Tel.: +39 011 090 3422x4638; fax: +39 011 090 3401x4699.
E-mail addresses: annalisa.chiappone@polito.it (A. Chiappone), claudio.gerbaldi@iit.it, claudio.gerbaldi@polito.it (C. Gerbaldi).

0378-7753/$ – see front matter © 2011 Elsevier B.V. All rights reserved.
doi:10.1016/j.jpowsour.2011.07.015

consist of alternating crystals and amorphous strings showing a web-like structure [19]. Due to their high aspect ratio and mechanical properties, MFCs have already been used as rheology modifier in food, paints, cosmetics, pharmaceutical products and as reinforcing agent in polymer nanocomposites giving excellent results [19–21]. Recently, MFCs have also been used as binder for the aqueous processing of cellulose–graphite nanocomposite electrodes for flexible paper-like Li-ion batteries [22] and studied as reinforcement for PEO based solid polymer electrolytes [23].

In the field of nanocomposites, the method of in situ polymerisation has given the most interesting results [24]. However, free radical photo-polymerisation (UV-curing) is a promising approach for the production of nano- and micro-composite thermo-set polymer coatings, inks adhesives and membranes where the surface to volume ratio is high. It takes place at room temperature under UV light and is an easy and reliable process [25]. UV curing gives a very fast and low-cost production process with an environmentally friendly approach, as the use of solvents is avoided. Considering the interesting properties of MFCs and the potentials of free radical photo-polymerisation, a UV-cured MFC-polymer composite membrane could surely give outstanding results if applied to flexible batteries, where improved mechanical properties are fundamental. In this scenario, the present work illustrates the possibility of using the photopolymerisation process to prepare composite methacrylic-based thermo-set gel-polymer electrolyte (GPE) membranes, a class of reinforced polymeric networks obtained by incorporating microfibrillated cellulose particles into a methacrylic-based polymer matrix. Such modification would make these hybrid organic, green, cellulose-based systems a strong contender in the field of thin flexible Li-based power sources. The promising perspectives of such kind of GPEs are illustrated by the experimental data on the electrochemical response of a laboratory-scale lithium polymer cell.

2. Experimental

2.1. Materials

Bisphenol A ethoxylate (15 EO/phenol) dimethacrylate (BEMA, average M_n: 1700), and poly(ethylene glycol) methyl ether methacrylate (PEGMA, average M_n: 475) were obtained from Sigma–Aldrich. 2-Hydroxy-2-methyl-1-phenyl-1-propanon (Darocur 1173) from Ciba Specialty Chemicals was used as the free radical photo-initiator. The 1.0 M $LiPF_6$ in EC/DEC (1:1, w w^{-1}) solution (battery grade) was obtained from Ferro Corp., USA.

The $LiFePO_4$/C cathode material was synthesized in the form of nanostructured powder through a mild hydrothermal procedure developed at Politecnico di Torino and described in details elsewhere [26,27]. Lithium metal foils with a thickness of 200 μm were obtained from Chemetall.

Before their use, BEMA and PEGMA were kept open in the inert atmosphere of a dry glove box (MBraun Labstar, O_2 and H_2O content < 0.1 ppm) filled with extra pure Ar 6.0 for several days and, also, treated with molecular sieves (Molecular sieves, beads 4 Å, 8–12 mesh, Aldrich) to ensure the complete removal of traces of water/moisture from the liquid monomers.

2.2. Microfibrillated cellulose (MFC) nanoparticles preparation

MFC nanoparticles were prepared by treating bleached cellulose fibres at high pressure in a microfluidizer processor (Microfluidics, model M-110 EH-30) with a 400 and 200 μm diameter chamber. Cycles were varied in order to optimize the fibrillation process. The detailed procedure has been already described elsewhere [28]. A MFC aqueous suspension (1 wt.%) was prepared in the present work.

2.3. Composite gel-polymer electrolyte (GPE) membranes preparation

A BEMA:PEGMA reactive mixture was prepared in 50:50 ratio, along with 2 wt.% of free radical photo-initiator. The MFC suspension was added to the reactive formulation in different ratios in order to obtain composites containing 1, 3, 5 wt.% of MFC. As MFC aqueous suspensions are inherently stable, no sonication step was necessary. The liquid mixture was left 24 h in an oven at 70 °C to obtain the water evaporation and, subsequently, UV cured for 3 min under N_2 flux by using a medium vapour pressure Hg lamp (Helios Italquartz, Italy), with a radiation intensity on the surface of 30 mW cm^{-2}. Later, self standing films were peeled off from the glass plates and treated in high vacuum at 80 °C overnight. The samples were then stored in the dry glove box. Finally, the composite polymer membranes were activated by soaking them into the liquid electrolyte swelling solution for about 2 h to obtain the gel-polymer electrolytes.

By the above-explained method we were able to produce flexible and easy to handle films, with a final thickness of about 150–200 μm (measured with a Mitutoyo series 547 thickness gauge equipped with an ABSOLUTE Digimatic Indicator model ID-C112XBS, with a resolution of ±1 μm and a max measuring force of 1.5 N), and an active swelling percentage approaching 50 wt.%.

2.4. SEM analysis

Morphological characterization of the samples was performed employing a FEI Quanta Inspect 200LV scanning electron microscope (SEM, max magnification of 1.5×10^5) equipped with an Everhardt Thornley secondary electron detector (ET-SED). Prior to analysis, all the samples were coated with a thin Cr layer (thickness around 10 nm) to minimize the effect of the electron beam irradiation which may possibly lead to charging and "burning" of the polymer network. Top analysis was performed in order to evaluate qualitatively the MFC dispersion. Moreover, test membranes were cracked under cryogenic conditions (after dipping in liquid nitrogen in order to avoid any change in the morphology) and a cross-sectional analysis was performed to estimate the uniformity of MFC filling across the membrane thickness.

2.5. Determination of the cross-linked fraction (gel-content)

The insoluble fraction (gel content) of the cured products was determined as described in the following, according to the standard test method ASTM D2765-84. The samples were held in a metal net, accurately weighed, and subsequently extracted with $CHCl_3$ to dissolve the non cross-linked polymer chains. Extraction included 24 h of residence time for the solvent to appeal the membranes at room temperature. The cross-linked fraction was then calculated by dividing the mass of the dry sample left after the extraction by the calculated mass of the original sample (relative error = ±1%).

2.6. Thermal analysis

The glass transition temperature (T_g) of the materials was evaluated by differential scanning calorimetry (DSC) with a METTLER DSC-30 (Greifensee, Switzerland) instrument, equipped with a low temperature probe. Samples were put in aluminium pans, prepared in the dry glove box. In a typical measurement, the electrolyte samples were cooled from ambient temperature down to −140 °C and, then, heated at 10 °C min^{-1} up to 120 °C. For each sample, the same heating module was applied and the final heat flow value was

recorded during the second heating cycle. The T_g was defined as the midpoint of the heat capacity change observed in the DSC trace during the transition from glassy to rubbery state. The thermal stability was tested by thermo-gravimetric analysis using a TGA/SDTA-851 instrument from METTLER (Switzerland) over a temperature range of 25–600 °C under N_2 flux at a heating rate of 10 °C min^{-1}.

2.7. Mechanical properties

Mechanical measurements on the polymer membranes before swelling were carried out through tensile experiments according to ASTM Standard D638, using a Sintech 10/D instrument equipped with an electromechanical extensometer (clip gauge). At least five specimens for each sample were tested; the standard deviation in Young's modulus (E) was 5%. Mechanical properties after swelling were evaluated by a bending test for which the membranes were rolled up around cylindrical hoses with radii ranging between 3 and 32 mm.

2.8. VIS spectroscopy

Transmittance measurement were carried out by using a double beam UNIVAM UV2 (ATI Unicam, Cambridge, UK) spectrophotometer with variable slit width in the spectral range from 400 to 800 nm, interfaced to a computer via "Vision 32" software for data elaboration.

2.9. Ionic conductivity measurements

The ionic conductivity tests of the polymer electrolyte membranes were carried out by electrochemical impedance spectroscopy (EIS) analysis on a heating stepped ramp from 20 °C to 80 °C. The test cells (model ECC-Std, http://el-cell.com/products/test-cells/ecc-std, purchased from EL-Cell GmbH), formed by sandwiching discs of 2.54 cm^2 of the given membrane between two stainless-steel blocking electrodes, were housed in a Memmert GmbH oven model UFE-400 with a temperature control of ±1 °C. The resistance of the electrolyte was given by the high frequency intercept determined by analysing the impedance response using a fitting program provided with the Electrochemistry Power Suite software (version 2.58, Princeton Applied Research). Each sample was equilibrated at the experimental temperature for about 1 h before measurement, to allow thermal equilibration of the cells. All measurements were carried out on at least three different fresh samples in order to verify the reproducibility of the obtained results.

2.10. Electrochemical stability measurements

The electrochemical stability window (ESW) was evaluated at ambient temperature by linear sweep voltammetry in three electrode cells (model ECC-Ref, http://el-cell.com/products/test-cells/ecc-ref) using an Arbin Instrument Testing System model BT-2000. Separate tests were carried out on each polymer electrolyte sample to determine the cathodic and anodic stability limits. The measurements were performed by scanning the cell voltage from the OCV towards 0.0 V vs. Li (cathodic scan) or 5.5 V vs. Li (anodic scan). In both cases, lithium metal has been used as the reference electrode and the potential was scanned at a rate of 0.100 mV s^{-1}. The current onset of the cell was associated with the decomposition voltage of the electrolyte. Cell configuration adopted for anodic scan: acetylene black (Shawinigan Black AB-50, Chevron Corp., USA) over Al current collector and Li metal as electrodes and the given membrane as electrolyte (active area equal to 2.54 cm^2); cathodic scan: Cu foil and Li metal as electrodes and the given membrane as electrolyte (active area equal to 2.54 cm^2).

2.11. Lithium polymer cell assembly and electrochemical tests

The lithium polymer cell was assembled by contacting in sequence a lithium metal disk anode, a layer of the nanocomposite gel-polymer electrolyte and a $LiFePO_4$/C disk composite cathode (electrode area: 2.54 cm^2). The latter was prepared by a quick and low cost mild hydrothermal synthesis as described in a previous work [26]. The electrodes/electrolyte assembly was housed in an Electrochemical Test Cell (model ECC-Std). Both electrode fabrication and cell assembly were performed in the environmentally controlled dry glove box. The lithium cell was tested for its electrochemical behaviour at room temperature in terms of charge/discharge galvanostatic cycling using an Arbin Instrument Testing System model BT-2000. The voltage cut-offs were fixed at 4.0 V vs. Li/Li$^+$ (charge step) and 3.0 V vs. Li/Li$^+$ (discharge step), respectively.

3. Results and discussion

3.1. Composite polymer membranes (electrolyte-free)

Liquid electrolyte-free polymer membranes were prepared by photo-copolymerising the di-functional methacrylic oligomer BEMA and the mono-functional PEGMA with the in situ addition of microfibrillated cellulose. Table 1 shows the composition of the various salt-free solid polymer membranes. A MFC-free sample, named MFC-0, was made of BEMA and PEGMA in 50:50 ratio. BEMA was chosen because it is well known that can be readily polymerised by UV-curing, thus forming a cross-linked homopolymeric network. PEGMA, usually referred as reactive diluent, is meant to be useful to increase the mobility of Li$^+$ ions inside the polymer matrix along with an enhancement in the ionic conductivity through its pendant ethoxy groups. Detailed characteristics of these and other similar systems can be found in previous works [29–33].

The polymer membranes obtained copolymerising the monomers BEMA and PEGMA with the in situ addition of microfibrillated cellulose particles are freestanding, extremely flexible and non-sticky. An example is shown in Fig. 1, which illustrates the appearance of the MFC-3 composite polymer membrane, representative for all the samples prepared.

In the absence of the filler the polymer is transparent, while it progressively becomes opaque by increasing the amount of MFC. Measurements performed by a visible spectrophotometer showed that transmittance decreases when the cellulose particles percentage is increased (see Table 1).

The characterisation of the UV-cured films included the evaluation of the gel content, differential scanning calorimetry, thermo-gravimetric analyses, mechanical tests and SEM analyses. The conversion of the monomers after photopolymerisation was evaluated by measuring the gel-content: it showed a decrease of the cross-linking in the presence of higher quantities of MFC. The obtained values are reported in Table 1. One possible explanation for such behaviour may be the hindrance of UV light penetration inside the polymeric network associated with the increased presence of particles; in fact, as MFC are crystalline materials with a length of few microns, they may hinder the penetration of the light inside the polymer bulk.

The glass transition temperature (T_g) was evaluated by differential scanning calorimetry (DSC) and the results obtained are shown in Fig. 2. DSC measurements were performed on the MFC-0 matrix and related MFC reinforced composites. All the characteristic temperatures of the studied films are summarized in Table 1. The T_g

Table 1
Brief summary of the most relevant features of the electrolyte-free composite polymer membranes.

Sample	BEMA:PEGMA ratio	MFC content (wt.%)	Gel-content (%)	Transmittance 400–800 nm (%)	T_g (°C)	$T_{5\%}$ (°C)	$T_{10\%}$ (°C)
MFC-0	50:50	0	93	87	−56.2	225	285
MFC-1	50:50	1	92	42	−53.2	249	286
MFC-3	50:50	3	82	10	−53.7	265	300
MFC-5	50:50	5	80	7	−53.4	275	312

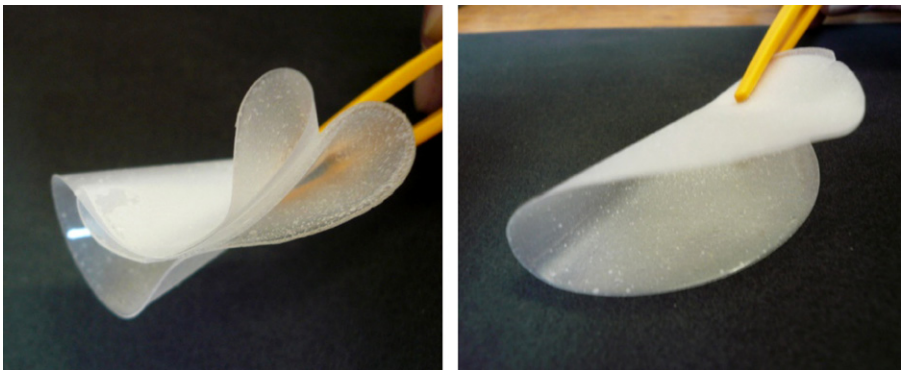

Fig. 1. Appearance of the MFC-3 composite polymer membrane obtained by copolymerising the monomers BEMA and PEGMA in 50:50 ratio via UV irradiation, with the in situ addition of 3 wt.% of MFC in aqueous suspension.

was defined as the midpoint of the heat capacity change observed in the DSC trace during the transition from glassy to rubbery state. The differential scanning calorimetry analyses evidenced T_g values lower than −50 °C for all the samples prepared, indicating that at room temperature the polymer membranes are in a rubbery state. As clearly depicted in Fig. 1, though the T_g is very low, the membranes are self-standing, extremely flexible and easy to handle. The different percentage of the filler in the polymer matrix does not significantly influence the DSC trace and, consequently, the final characteristics of the films; indeed, the T_g values in presence of the filler are increased only of few degrees (see Table 1), meaning that there is not much interaction between the filler particles and the amorphous polymer segments.

The thermal stability of the prepared membranes was assessed by thermo-gravimetric analysis under flowing nitrogen in the temperature range between 25 °C and 600 °C. The results are shown in Fig. 3 and summarized in Table 1. The stability was very high over a wide range of temperatures; a one-step weight loss process with the detection of noticeable change only at above 275 °C was observed. The increase in the MFC content led to an increase in the stability of the polymers. The degree of activity of the additives was rated on the basis of the temperatures for 5% and 10% weight loss, i.e., $T_{5\%}$ and $T_{10\%}$ (see Table 1).

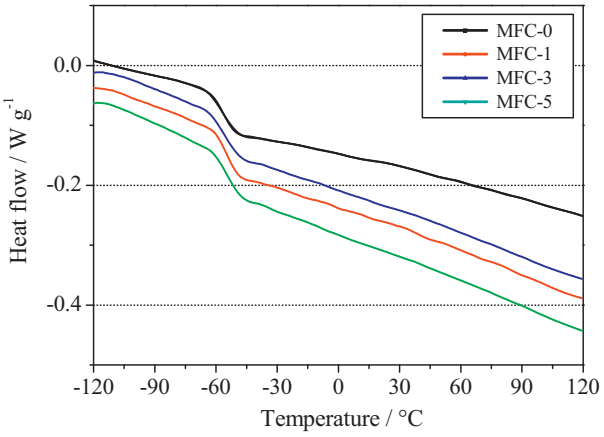

Fig. 2. DSC traces of the series of composite polymer membranes prepared.

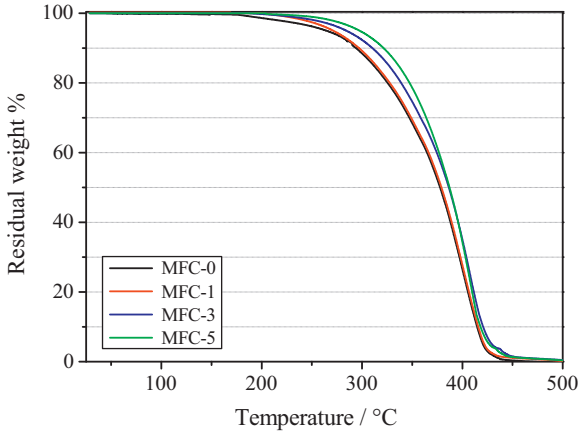

Fig. 3. TGA measurements on the composite polymer membranes: the presence of MCFs slightly improves thermal stability.

The mechanical behaviour of the electrolyte-free MFC polymer composites was investigated to compare the effect of the amount of cellulosic filler on the mechanical properties of the resulting membrane (see Fig. 4 and Table 2). Compared to the previously prepared membranes [29,30], which already had good thermal and electrochemical properties, these composite polymer membranes showed an important improvement in mechanical properties obtained by means of tensile test studies. The addition of microfibrils can widely increase the Young's modulus and the tensile resistance, leading to values that are highly satisfactory for the possible application in

Table 2
Young's modulus and resistance to traction of the composite polymer membranes.

Sample	Young's modulus (MPa)	σ max (MPa)
MFC-0	12 ± 2	0.5 ± 0.35
MFC-1	20 ± 3	0.9 ± 0.4
MFC-3	42 ± 4	2.1 ± 0.6
MFC-5	79 ± 6	3.5 ± 0.3

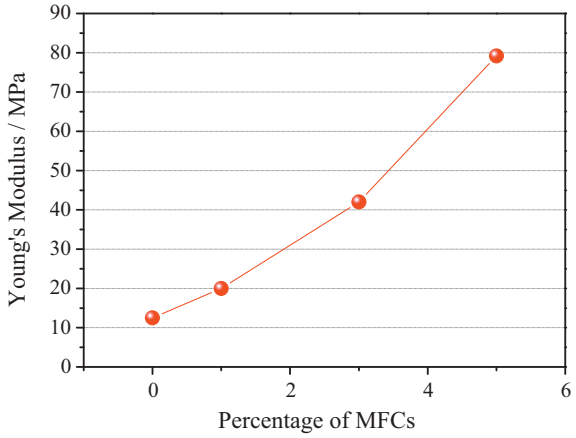

Fig. 4. Plot of Young's modulus vs. the quantity of filler.

thin flexible batteries. Such an excellent mechanical behaviour may also improve the safety features of the resulting GPE membranes; in fact the cellulose fibres, being highly crystalline and very strong, can block the growth of lithium dendrites and drastically reduce the possibility of short circuits.

The morphology of the MFC composite polymers was characterised by SEM analysis. SEM micrographs were obtained, for both surfaces and cross-sections, on all the samples in order to observe the dispersion of MFCs into the polymer matrix. Some examples are shown in Fig. 5, illustrating that MFCs were uniformly dispersed, whatever the spot probed in the sample. The composite appear highly homogeneous, showing a complete interpenetration between fibres network and polymer: cellulose microfibrils are completely covered by the polymer matrix. In Fig. 6 the cross-sectional images, at different magnification, of the sample with 3% of MFC is shown. A good affinity between the matrix and the filler was obtained even without functionalization of MFCs. This could be attributed to the good compatibility resulting from the chemical similarities between polymer and MFCs and, consequently, the hydrogen bonding interactions existing at the interface. For all the composite samples, it was observed a homogeneous dispersion of white dots that were associated with the presence of microfibrils. These white dots do not correspond to isolated particles since the particle dimensions were too small to be observed at this scale. As already reported by Dufresne and co-workers [34,35], the white dots result from charge concentration effects due to the emergence of cellulose microfibrils from the observed surface, which increase the apparent cross-section of MFCs present over the surface. It is worth noting that white dots are homogeneously dispersed within the polymer matrix with no apparent formation of large aggregates, suggesting good compatibility between fillers and matrix. Such uniform distribution of the fillers in the matrix could play an important role in improving the mechanical performance of the resulting nanocomposite films.

Table 3
Active swelling percentage (AS%) is calculated as [(Wf – Wi)/Wf] × 100, where Wf is the weight of the membrane after swelling and Wi is the weight before swelling. It indicates the percentage of electrolyte solution uptaken during the swelling process.

Sample	Active Swelling (AS%)	σ @ RT (S cm^{-1})	σ @ 80 °C (S cm^{-1})
MFC-0	53.0	1.1×10^{-3}	7.0×10^{-3}
MFC-1	55.0	6.4×10^{-4}	3.1×10^{-3}
MFC-3	58.5	8.4×10^{-4}	4.4×10^{-3}
MFC-5	57.0	7.7×10^{-4}	4.9×10^{-3}

3.2. Composite gel-polymer electrolyte (GPE) membranes

The composite membranes were swelled in the electrolyte solution made of 1.0 M $LiPF_6$ in EC/DEC (1:1, w w^{-1}). The electrolyte uptake, called Active Swelling percentage (AS%), was calculated by the formula:

$$\frac{Wf - Wi}{Wf} \times 100$$

where Wf is the weight of the membrane after swelling and Wi is the weight before swelling). It was estimated to be approximately 55 wt.% for all the samples (Table 3).

Even after swelling, the membranes containing MFC showed better dimensional stability and mechanical behaviour. Fig. 7 shows the aspect of the membranes after swelling (in particular, Fig. 7A the MFC-0 electrolyte membrane, while Fig. 7B the MFC-3 electrolyte membrane). The bending test performed on the membranes MFC-0 and MFC-3 after swelling for 2 h in a EC:DEC (1:1) mixture demonstrated that the MFC-3 membrane can still be easily rolled up on the cylinders used for the test withstanding all the bending radius till 3 mm. On the contrary, the membrane without microfibrils was difficult to handle and it failed if bended on a cylinder with a 10 mm radius. Also the dimensional stability of the membrane was found to be remarkably higher in the presence of the filler; in fact, after swelling the MFC-0 membrane showed an increase in volume of 35%, while for the MFC-3 was only 20%.

The thermal stability of the membrane MFC-3 after swelling was evaluated by TGA analysis, the resulting curve is shown in Fig. 8, where it is compared to the curve obtained before swelling. The electrolyte evaporated quite quickly under the measurement con-

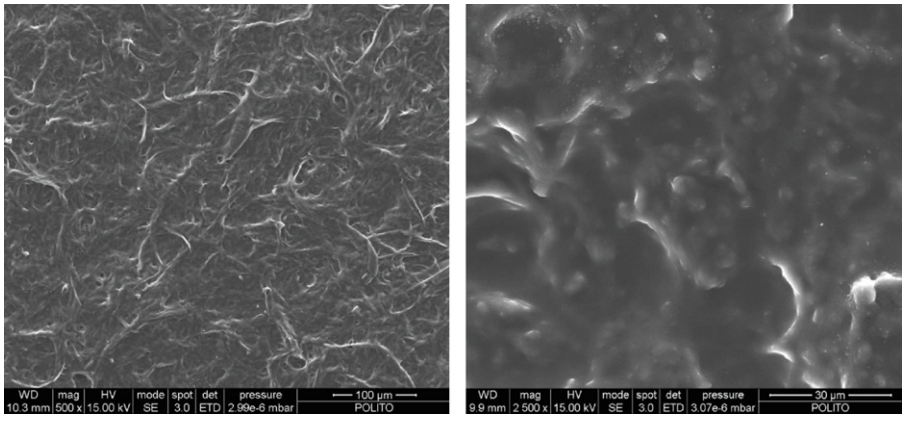

Fig. 5. SEM images of the composite polymer membrane MFC-3 at different magnitudes: 500× left and 2500× right. It is possible to observe that the cellulose microfibrils are completely surrounded by the polymer matrix.

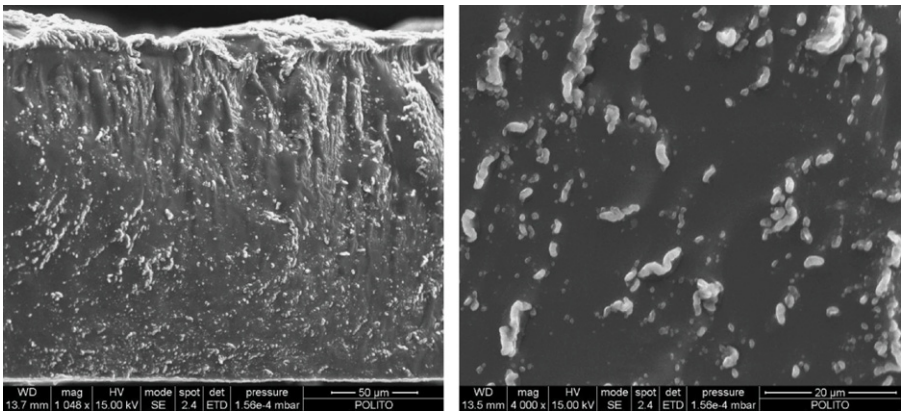

Fig. 6. Cross-sectional SEM images of the composite polymer membrane MFC-3 at different magnitudes: ~1000× left and 4000× right.

ditions (N_2 flux of 60 ml min^{-1}); the $T_{5\%}$ temperature was reached at around 90 °C. It is possible to observe that the complete evaporation of the organic solvent, which was considered at 250 °C, confirmed the active swelling percentage of 55%; at temperatures higher than 250 °C it is possible to observe the decomposition of the polymer composite. While the unswelled membrane showed a residue at high temperature of about 2.7%, which was completely attributable to the presence of cellulose ashes, in the case of the swelled membrane the residue had higher values (i.e., 5.4%) that was explainable considering the presence of the lithium salt.

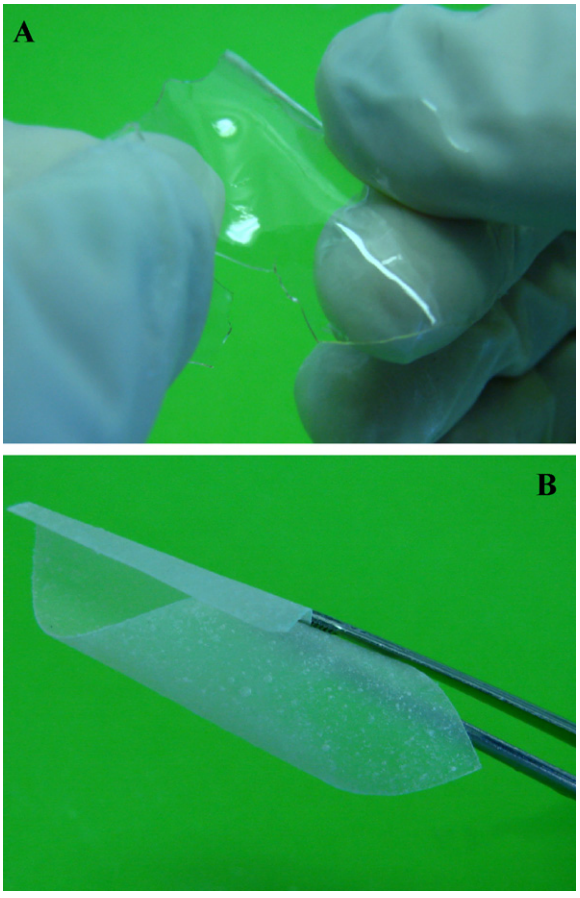

Fig. 7. Appearance of the MFC-3 (A) and MFC-0 (B) composite gel-polymer membranes. After a 2 h swelling time, the BEMA:PEGMA membrane could be hardly handled while the MFC-3 was easily bendable.

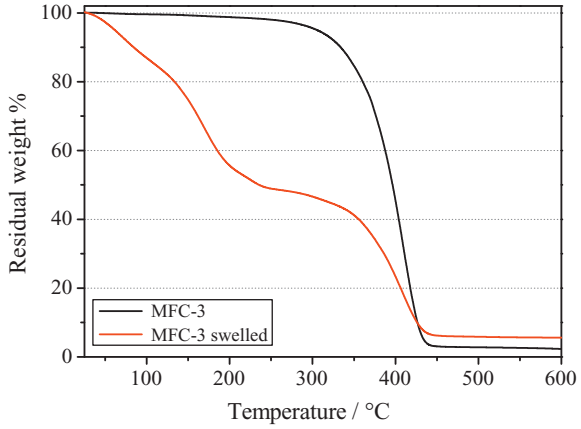

Fig. 8. TGA measurements on the MFC-3membrane before and after swelling.

3.3. Ionic conductivity

In view of their application in lithium batteries, we first screened the samples by determining their ionic conductivity. The ionic conductivity of all the samples was evaluated by impedance spectroscopy after swelling for 2 h in a 1.0 M $LiPF_6$ solution in EC:DEC (1:1). The active swelling values are summarized in Table 3. Fig. 9 shows the impedance response, in the form of Nyquist plots, of four independent cells formed by sandwiching the given elec-

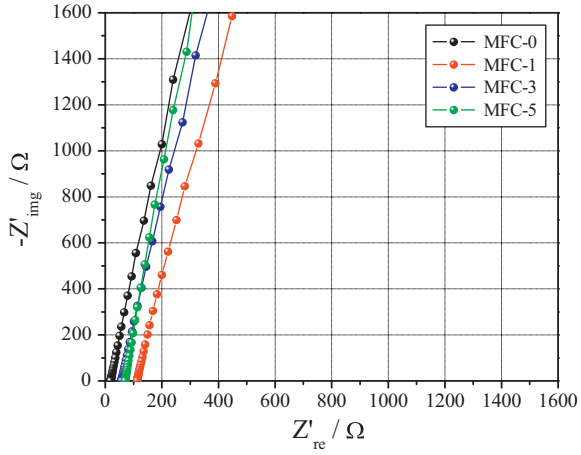

Fig. 9. Typical impedance response of the four gel-polymer electrolyte membranes developed in this study. Stainless-steel blocking electrodes. Frequency = 1 Hz–100 kHz.

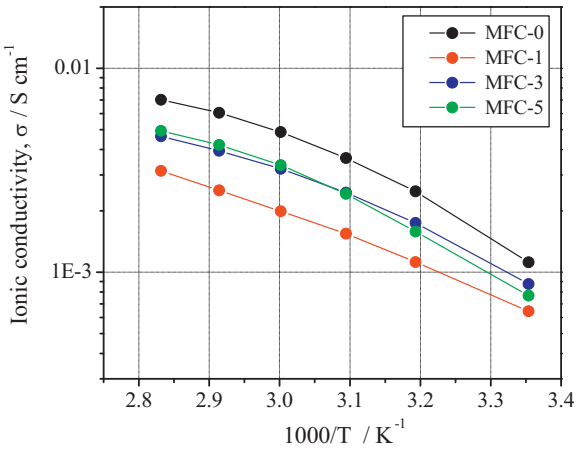

Fig. 10. Ionic conductivity Arrhenius plots of the four nanocomposite polymer electrolytes developed in this work. Data obtained from impedance spectroscopy.

trolyte membrane sample between two blocking stainless-steel electrodes, recorded after one week of storage at room temperature. The intercepts with the real axis allow calculation of the conductivity values of the membranes. Notably, in the whole investigated frequency range, no signs of charge transfer or passivating layer formation are detectable. A linear response, as typically expected for blocking electrodes, indicates that our membranes do not undergo unexpected collateral reactions or undesired phenomena when placed in contact with the stainless steel electrodes.

Fig. 10 shows the temperature dependence of the ionic conductivity of the membranes in the form of Arrhenius plots. The MFC-0 sample displayed the highest conductivity in the whole range of temperatures investigated in this study, attaining values in the order of 10^{-2} S cm^{-1} at 80 °C. As clearly visible, the membranes containing the filler showed a slightly lower conductivity, in particular MFC-1, while MFC-3 and MFC-5 behave almost in the same way. The ionic conductivities of the MFC membranes are about 6×10^{-4} S cm^{-1} at room temperature and they increase with the increase of the temperature, reaching a high value of about 3×10^{-3} S cm^{-1} at 80 °C. The regular increase in conductivity upon heating is observed for all the membranes and confirms that neither physical transitions nor segregation phenomena occurred during the test. Moreover, all impedance spectra obtained in the selected temperature range do not show any sign of high-frequency semicircles which could indicate lack of gel homogeneity due to crystalline phase separation.

It is also possible to see from the Arrhenius plots that the conductivity behaviour of the samples MFC-3 and 5 is the most similar to the MFC-0 one, while the worst values are given by the sample MFC-1. Such a result could be due to the lower polymerisation level of the samples MFC-3 and 5 indicated in Table 1 by means of gel content. A lower conversion of the oligomers leads to a more mobile network and, moreover, the unreacted monomers can be easily replaced by the swelled electrolyte.

3.4. Electrochemical stability window (ESW)

In general, for a lithium battery, the anodic reaction occurs in the vicinity of 0 V vs. Li/Li$^+$, while the cathode potentials can approach values as high as 4.5 V vs. Li/Li$^+$, implying that the electrochemical stability window (ESW) is a fundamental parameter regarding cycling reversibility. The ESW of the MFC-3 composite polymer electrolyte (representative for all the samples prepared) measured at ambient temperature is depicted in Fig. 11A and B. In fact, independently of the amount of MFC added, all samples exhibited a wide ESW ranging from the lithium plating to around 5.0 V vs. Li/Li$^+$. The

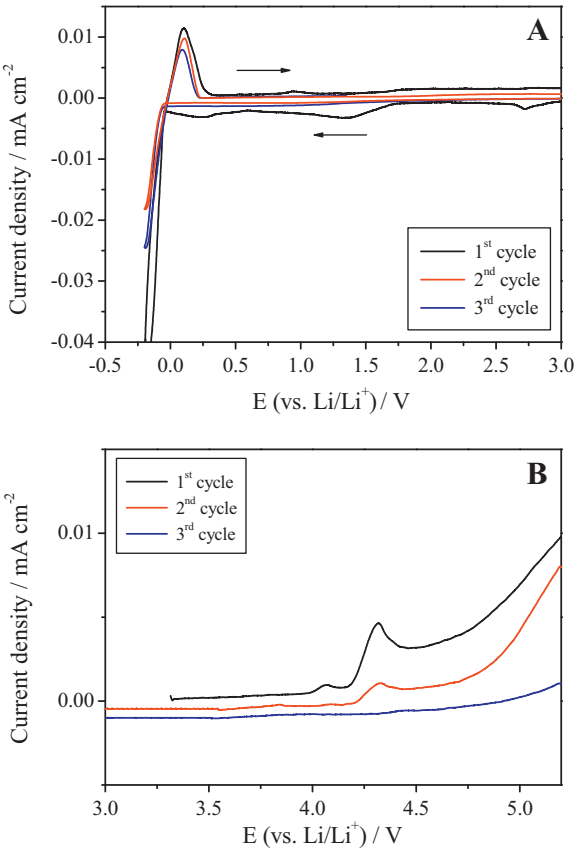

Fig. 11. Electrochemical stability window (ESW) of MFC-3 at 25 °C; potential scan rate of 0.100 mV s^{-1}. (A) Electrochemical stability window in the cathodic voltage range and (B) electrochemical stability window in the anodic voltage range.

cathodic stability was evaluated by running a sweep voltammetry of a cell using a copper working electrode and a lithium metal counter electrode. The resulting current–voltage traces (Fig. 11A) showed in the first sweeping cycle a current flow at about 2.7 V vs. Li/Li$^+$, followed by a large current flow starting at around 1.5 V. The first event is most probably due to some decomposition of the cellulosic material, while the latter is associated with a multistep decomposition process, very likely due to the reduction of the carbonate solution component, with the consequent formation of a passivating film on the testing electrode. This interpretation is supported by a series of findings, such as: (a) the irreversibility of the peaks, and (b) the trend of the second sweep cycle where no marked trace of events is detected. The current flow in the 0.25 V voltage range can be ascribed to another sort of "passivation" phenomenon, as the peak is clearly visible during the first cycle which immediately disappears with subsequent cycling. As a whole, the figure illustrates a cathodic scan starting from the open-circuit voltage and extending down to the lithium deposition range, i.e., to −0.2 V vs. Li/Li$^+$. The lithium deposition–lithium stripping peaks on and from the copper substrate are clearly visible [36].

The increase of the current during the first anodic scan, which is related the decomposition of the electrolyte, was taken in correspondence to the onset of a low current peak at approx. 4.3 V vs. Li/Li$^+$. However, even if the current rises at a lower voltage, after few cycles its trend consistently deviates from that observed in the first cycle, showing a sort of "passivation" phenomenon which extends the anodic stability up to higher voltage, i.e., above 5 V vs. Li/Li$^+$. This behaviour has already been observed in previous studies concerning polymer electrolytes reinforced by cellulose [37].

Three important features can be derived by the ESW results, namely: (a) the anodic onset of the current is detected at around

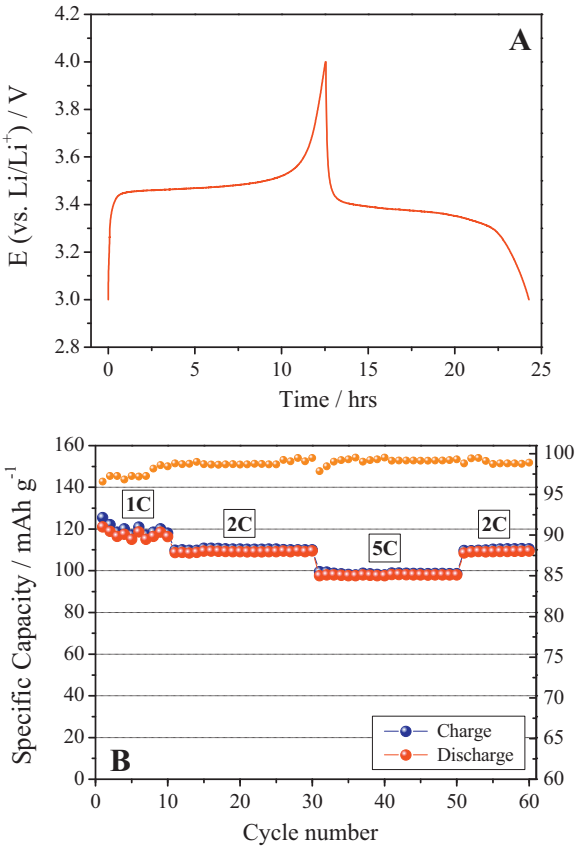

Fig. 12. (A) Typical charge and discharge cycle run at ambient temperature. (B) Specific capacity vs. cycle number of the lithium cell assembled by contacting in sequence the $LiFePO_4$ composite cathode, the MFC-3 membrane and a Li metal anode, at ambient temperature and at different current rates from 1 C to 5 C.

5 V vs. Li/Li^+, which is assumed as the membrane decomposition voltage, i.e., a value high enough to allow a safe use of the membrane in connection with Li-ion electrode couples which typically cycle above 3.5 V; (b) the occurrence of a reversible cathodic peak around 0 V related to the lithium deposition-stripping process on the copper electrode, which demonstrates the applicability of these membranes for lithium rechargeable batteries; and (c) the very flat current–potential curves between the two limits, which is a clear evidence of the purity and of the integrity of the membranes and the synthesis method adopted.

3.5. Lithium cell electrochemical testing

High ionic conductivity and wide electrochemical stability window are highly welcomed properties in battery applications; hence, we selected the MFC-3 membrane and concentrated our attention on this membrane for further characterization. A laboratory scale lithium cell was assembled by combining a lithium metal anode with a $LiFePO_4$/C cathode and using the MFC-3 as the electrolyte and tested in order to evaluate the capability of the electrolyte to perform in a real battery configuration. Its electrochemical behaviour was investigated by means of galvanostatic charge/discharge cycling performed at room temperature.

The electrochemical process of this battery is the reversible removal-uptake of lithium from and to lithium iron phosphate:

$$LiFePO_4 \leftrightarrow xLi + Li_{(1-x)}FePO_4$$

which is expected to develop along a 3.5 V vs. Li/Li^+ flat plateau for a total specific capacity of 170 mAh g^{-1}.

Fig. 12A illustrates a typical charge (lithium removal from $LiFePO_4$ to form $FePO_4$) and discharge (lithium acceptance by $FePO_4$ to reconvert into $LiFePO_4$) cycle run at ambient temperature. Fig. 12B shows the specific capacity vs. cycle number at ambient temperature and at different current rates from 1 C to 5 C (1 C = 0.7 mA with respect to a $LiFePO_4$ active mass of about 4 mg). Reproducible voltage profiles were obtained where the initial specific capacity approaches the value of 120 mAh g^{-1} at 1 C The capacity retention is satisfactory: at high 5 C current rate the cell still delivers specific capacity values around 100 mAh g^{-1}, with a drop in capacity of less than 18% with respect to the initial value at 1 C. The battery operates with the expected voltage profiles delivering a good fraction of the theoretical capacity even at rates as high as 5 C. The cycle response is also encouraging since no decay in capacity is shown during this initial test and the charge–discharge efficiency following the first cycles, where rearrangements in the structure of the electrode take place, is maintained to be always higher than 98%. Finally, it is important to note that the system behaves correctly, with no abnormal drift even at high regimes; in fact, reducing the C-rate completely restores the specific capacity (see, in Fig. 12B, the specific capacity values from 5 C to 2 C after the 50th cycle). The results here discussed, although preliminary, demonstrate the feasibility of the MFC reinforced membranes as a new electrolyte for advanced lithium polymer batteries.

4. Conclusions

Microfibrillated cellulose at a concentration of 1–5% by weight was used to reinforce methacrylic-based composite polymer electrolyte membranes prepared by UV-curing process. It has been shown that Young's modulus, tensile strength and thermal stability of the composite films increase with increasing the MFC contents. Mechanical properties and dimensional stability of the membranes after swelling in the electrolyte solution are also improved with the addition of microfibrils. The impedance spectroscopy performed on the composite GPEs showed high ionic conductivity values approaching 10^{-3} S cm^{-1} even at ambient temperature and the analysis of the electrochemical behaviour evidenced a wide stability window and interesting performance in real battery configuration.

These excellent results added to the easy preparation method and the low processing costs make MFCs a perfect candidate for the production of composite membranes that can be used as gel-polymer electrolytes for application in lithium-based thin flexible batteries and open further studies about the role of cellulose in ion conduction. It is here also confirmed that, compared to other techniques, UV curing is versatile due to its easiness and rapidity in processing. It can open up promising perspectives in obtaining innovative polymeric electrolytes with high flexibility, well suited for flexible and/or non-planar electronics application.

Acknowledgement

Authors would like to thank Mr. Mauro Raimondo for the SEM analysis of the samples.

References

[1] B. Scrosati, Chem. Rec. 5 (2005) 286–297.
[2] B. Scrosati, J. Garche, J. Power Sources 195 (2010) 2419–2430.
[3] A.S. Aricò, P. Bruce, B. Scrosati, J.M. Tarascon, W. Van Schalkwijk, Nat. Mater. 4 (2005) 366–377.
[4] I. Chung, I. Kang, Mol. Cryst. Liq. Cryst. 507 (2009) 1–17.
[5] E. Abad, S. Zampolli, S. Marco, A. Scorzoni, B. Mazzolai, A. Juarros, D. Gómez, I. Elmi, G.C. Cardinali, J.M. Gómez, F. Palacio, M. Cicioni, A. Mondini, T. Becker, I. Sayhan, Sens. Actuators B: Chem. 127 (2007) 2–7.
[6] J.M. Tarascon, M. Armand, Nature 414 (2001) 359–367.
[7] E.J. Cairns, P. Albertus, Ann. Rev. Chem. Biomol. Eng. 1 (2010) 299–320.

[8] N. Terada, T. Yanagi, S. Arai, M. Yoshikawa, K. Ohta, N. Nakajima, A. Yanai, N. Arai, J. Power Sources 100 (2001) 80–92.
[9] B.V. Ratnakumar, M.C. Smart, C.K. Huang, D. Perrone, S. Surampudi, S.G. Greenbaum, Electrochim. Acta 45 (2000) 1513–1517.
[10] A. Dufresne, Molecules 15 (2010) 4111–4128.
[11] D. Nabi Saheb, J.P. Jog, Adv. Polym. Technol. 18 (1999) 351–363.
[12] I. Sirò, D. Plackett, Cellulose 17 (2010) 459–494.
[13] M.A.S. Azizi Samir, F. Alloin, A. Dufresne, Biomacromolecules 6 (2005) 612–626.
[14] M.A. Hubbe, O.J. Rojas, L.A. Lucia, M. Sain, BioResources 3 (2008) 929–980.
[15] A. Šturcova, G.R. Davies, S.J. Eichhorn, Biomacromolecules 6 (2005) 1055–1061.
[16] S.J. Eichhorn, A. Dufresne, M. Aranguren, N.E. Marcovich, J.R. Capadona, S.J. Rowan, C. Weder, W. Thielemans, M. Roman, S. Renneckar, W. Gindl, S. Veigel, J. Keckes, H. Yano, K. Abe, M. Nogi, A.N. Nakagaito, A. Mangalam, J. Simonsen, A.S. Benight, A. Bismarck, L.A. Berglund, T. Peijs, J. Mater. Sci. 45 (2010) 1–33.
[17] F.W. Herrick, R.L. Casebier, J.K. Hamilton, K.R. Sandberg, J. Appl. Polym. Sci.: Appl. Polym. Symp. 37 (1983) 797–813.
[18] A. Turbak, F. Snyder, K. Sandberg, U.S. Patent 4,378,381 (1983).
[19] J. Lu, T. Wang, L.T. Drzal, Composites: Part A 39 (2008) 738–746.
[20] J. Sreekumar, M. Sain, BioResources 1 (2006) 1–5.
[21] M. Sain, K. Oksman, ACS Symp. Ser. 938 (2006) 2–8.
[22] L. Jabbour, C. Gerbaldi, D. Chaussy, E. Zeno, S. Bodoardo, D. Beneventi, J. Mater. Chem. 20 (2010) 7344–7347.
[23] F. Alloin, A. D'Aprea, N. Kissi, A. Dufresne, F. Bossard, Electrochim. Acta 55 (2010) 5186–5194.
[24] M. Trujillo, M.L. Arnal, A.J. Müller, E. Lardo, S. Bredeau, D. Bonduel, P. Dubois, Macromolecules 40 (2007) 6268–6276.
[25] C. Decker, Prog. Polym. Sci. 21 (1996) 593–650.
[26] G. Meligrana, C. Gerbaldi, A. Tuel, S. Bodoardo, N. Penazzi, J. Power Sources 160 (2006) 516–522.
[27] S. Bodoardo, C. Gerbaldi, G. Meligrana, A. Tuel, S. Enzo, N. Penazzi, Ionics 15 (2009) 19–26.
[28] G. Siqueira, J. Bras, A. Dufresne, Biomacromolecules 10 (2009) 425–432.
[29] J.R. Nair, C. Gerbaldi, G. Meligrana, R. Bongiovanni, S. Bodoardo, N. Penazzi, P. Reale, V. Gentili, J. Power Sources 178 (2008) 751–757.
[30] J.R. Nair, C. Gerbaldi, M. Destro, R. Bongiovanni, N. Penazzi, React. Funct. Polym. 71 (2011) 409–416.
[31] K.M. Abraham, M. Alamgir, J. Electrochem. Soc. 137 (1990) 1657–1658.
[32] K.M. Abraham, M. Alamgir, Chem. Mater. 3 (1991) 339–348.
[33] H.S. Choe, B.G. Carroll, D.M. Pasquariello, K.M. Abraham, Chem. Mater. 9 (1997) 369–379.
[34] M.A.S. Azizi Samir, F. Alloin, J.-Y. Sanchez, A. Dufresne, Polymer 45 (2004) 4149–4157.
[35] M.N. Anglés, A. Dufresne, Macromolecules 33 (2000) 8344–8353.
[36] P. Reale, A. Fernicola, B. Scrosati, J. Power Sources 194 (2009) 182–189.
[37] J.R. Nair, C. Gerbaldi, A. Chiappone, E. Zeno, R. Bongiovanni, S. Bodoardo, N. Penazzi, Electrochem. Commun. 11 (2009) 1796–1798.